

Sensorless Real-Time Reduced Order Model Based Adaptive Maximum Power Tracking Pitch Controller for Grid Connected Wind Turbines

Abilash Thakallapelli¹, Sudipta Ghosh¹, Sukumar Kamalasan^{1*}

¹ Electrical and Computer Engineering, UNC Charlotte, Charlotte, USA

* E-mail: skamalas@uncc.edu

Abstract: This paper presents a sensor-less maximum power tracking (MPT) pitch controller for grid connected Wind Turbine (WT). The main advantage of the proposed architecture is that the approach ensures smooth operation and thus minimizes the mechanical stress and damage on the WT during high wind speed and grid transient conditions. Simultaneously, it also: a) reduces transients in Point of Common Coupling (PCC) bus voltage, b) reduces rotor speed oscillations, and c) controls the output power of the wind turbine without exceeding its thermal limits. The approach can work without wind speed measurements. In order to consider the effect of grid variations at the PCC, the affected area in the grid is modeled as a study area (area of interest), and remaining area (external area) is modeled as frequency dependent reduced order model (FDROM). The reduced order model (ROM) is then used to estimate the reference speed. The proposed controller is designed using the error between actual speed of the generator and the reference speed, to ensure smooth operation and limit the speed and aerodynamic power at the rated values. The architecture is evaluated using wind farm integrated Kundur's two-area and IEEE-39 bus test systems using real-time digital simulator (RTDS).

1 Introduction

In recent years, the move towards eliminating fossil fuel dependency and embracing sustainable energy based power generation has increased interest in integrating renewable energy sources (RES) into the power grid. In 2016, WTG provided almost 6% of U.S. electricity generation (about 37% of electricity generation from RES) [1]. However, WTGs operate under varying wind conditions and depends on time and geographical location, which may be above or below rated values, thus varying their output power. During high wind speed conditions, the controller should limit the speed of the generator not crossing the rated value by limiting the rotation rate of the rotor, since pitch system contributes to 21.3% of the overall failure rate of wind turbines [2]. This can be achieved by controlling the blade pitch angle [3]. However, in practical systems, WTG operations are also influenced by the dynamics of the entire power grid. Thus, the design of WTG controllers should take into consideration of grid dynamics. Wind speed conditions are generally measured using anemometers, failure of which can cause deterioration in tracking performance. This should be addressed in the controller design as well [4].

Grid level interactions of the wind farms/turbines are generally controlled considering a constant voltage at the PCC even though electro-mechanical dynamics are included in such simulations. This ignores response of the wind farms with the electromagnetic transients in the grid. The effect is on the mechanical fatigue that happens on the wind generators. If one should design a controller considering grid dynamics, detailed Electro-Magnetic Transient (EMT) based grid models with dynamic models of WTG including DFIG are required. However, detail modeling of large scale power grid is impractical due to computational complexity [5]. In [5, 6], to reduce computational burden several model order reduction techniques based on linearized models have been developed, but these models are effective only during low-frequency oscillations. A possible method to reduce computational burden while retaining accuracy is to model part of WTG integrated grid (study area) in detail and the remainder of the network (external area) [7] as an equivalent. For this, the external area is modeled as a combination of low frequency (Transient Stability Assessment -TSA type) and high

frequency (FDNE type) equivalents. In TSA type, the network is formulated as an admittance matrix at the fundamental frequency, and the generators are aggregated and modeled in detail such that low-frequency electromechanical oscillations are preserved, whereas the high-frequency oscillations are preserved by FDNE.

In the literature, several WTG pitch control strategies for limiting the aerodynamic power and generator speed are proposed. An individual pitch control scheme with a proportional-integral (PI) controller with two resonant compensators is proposed in [8]. However, the PI controllers are designed based on a specific operating point. A pitch angle controller based on fuzzy logic is proposed in [9], in which generator output power and speed are used as input to the controller. However, determining exact fuzzy rules and membership functions for a dynamically changing conditions are considered. In [10], a fuzzy predictive algorithm coupled with conventional PI controllers is proposed for wind-turbine collective-pitch control. In [11], a method of nonlinear PI control for variable pitch wind turbine is proposed. The non-linearities and disturbances are evaluated and compensated using extended order state and perturbation observer. However, this method uses only one set of PI parameters for various speeds. Ref. [12] investigated determining the pitch angle when wind speed exceeds rated value using particle swarm optimization (PSO) and [13] proposed a method for blade pitch angle control using PID control.

In this paper, a novel sensor-less method for smoothly controlling the transients of WTG during high wind speed is introduced. The architecture uses an online dynamic network model of the power grid that is computationally tractable, to calculate reference speed for tracking. Then an adaptive controller is designed for smooth tracking and limiting the mechanical stress on the turbine. The control variables used are the algebraic error between the calculated reference speed and actual generator speed. For controller adaptation, a model identification method based on Recursive Least Square (RLS) method is also designed [14]. RLS identification is performed online to estimate the transfer function with the difference between the reference and actual speed as the process output and the controlling signal as the process input. Then using the identified transfer function, the controller gains of the controller are calculated online. If there is a change in operating point, the controller auto-tunes as the

transfer function is identified every sample time. This auto-tuning feature allows the proposed controller to provide an efficient way for adjusting the pitch angle during changing system operating conditions, as opposed to the conventional PI controller where gains are constant irrespective of the system conditions.

1.1 Contributions

The advantages of the proposed architecture are it,

- auto-tunes based on the wind speed and grid conditions and thus can higher precision.
- can be implemented in practical systems as the online grid models are computationally tractable.
- provides dynamic control capabilities as opposed to conventional controllers.
- can eliminate the requirement of anemometer.
- reduces mechanical stress on the turbine, voltage transients and speed oscillations.

1.2 Paper Organization

The rest of the paper is organized as follows. In section II the wind turbine and generator modeling are discussed. In section III, frequency dependent reduced-order modeling of the large power grid is discussed. Section IV discusses the proposed adaptive pitch controller and example case study. Section V discusses the implementation of TSA/FDNE and the proposed control architecture in Real-time Digital Simulator. Section VI discusses the real-time simulation results and section VII concludes the paper.

2 Wind Turbine and Generator Modeling

The variable speed WTGs are more frequently involved in providing grid reliability as they are more controllable, provides reactive power support and harvests optimum energy over a wide wind speed range [15]-[16]. In this paper, a two-mass variable speed model of WTG is designed and scaled up to represent 200 MW of rated power at the VSC interface transformer for modeling purposes.

2.1 The Wind Turbine

The mechanical power output (P_m) of the turbine in kW [17] can be represented as

$$P_m = C_p(\lambda, \beta) \frac{\rho A}{2} v_{wind}^3 \quad (1)$$

where $C_p(\lambda, \beta)$ is the coefficient of performance of the turbine which can be determined from the C_p vs λ curve for different blade pitch angle (β), λ is the tip speed, ρ is the density of air in kg/m^3 , A is the area swept by the turbine blades in m^2 , and v_{wind} is the velocity of the wind in m/s. From this, λ can be represented as [18, 19]

$$\lambda = \frac{R\omega_t}{v_{wind}} \quad (2)$$

where R and ω_t , are the radius of the turbine (m) and the rotational speed of the turbine (rad/s) respectively.

2.2 The Coefficient of Performance

The turbine coefficient of performance describes the power extraction efficiency of the WT and is generally less than 0.5. This can be represented as [20]

$$C_p(\lambda, \beta) = c_1 \left[\frac{c_2}{\lambda_i} - c_3\beta - c_4 \right] e^{-\frac{c_5}{\lambda_i}} + c_6\lambda \quad (3)$$

where

$$\frac{1}{\lambda_i} = \frac{1}{\lambda + 0.08\beta} - \frac{0.035}{\beta^3 + 1}$$

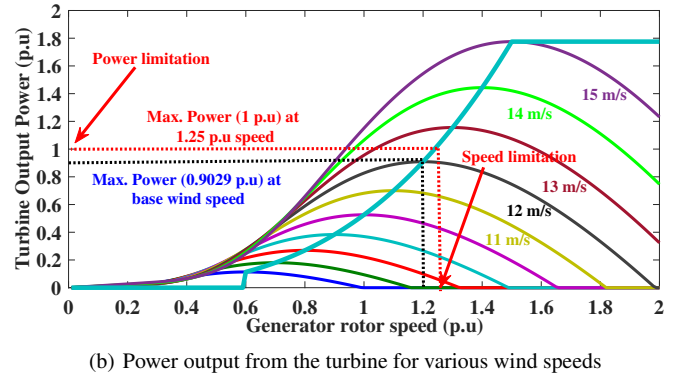
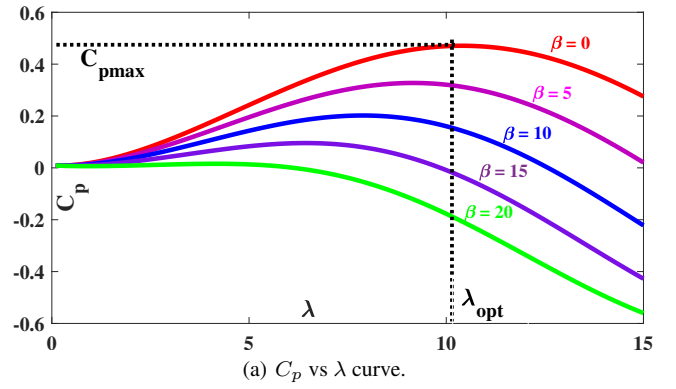


Fig. 1: Wind turbine characteristics.

For the proposed design, $c_1 = 0.5176$, $c_2 = 116$, $c_3 = 0.4$, $c_4 = 5$, $c_5 = 21$ and $c_6 = 0.0068$. The value of tip speed ratio λ is constant for all maximum power points. The maximum value for power coefficient C_p for a particular wind turbine can be obtained from C_p vs λ curve for different values of β . For the wind turbine selected for this work, the optimum value and the maximum value of λ are 10.4 and 0.48 respectively at $\beta = 0^\circ$. A characteristic plot of C_p vs λ for the proposed turbine based on (3) is as shown in Fig. 1(a). From Fig. 1(a), it can be observed that as β increases, λ decreases due to a decrease of turbine speed, and simultaneously C_p becomes less. This feature is used in pitch angle control to limit the speed of the rotor for wind speeds greater than the rated value. Fig. 1(b) shows the turbine output power (p.u) vs rotor speed (p.u) for various wind speeds.

2.3 Wind Generator

In the proposed study, type III DFIG with conventional vector control based Grid Side and Rotor Side Controllers is considered. The detailed nonlinear model of DFIG is developed in RSCADTM. Modeling details of DFIG are discussed in several previous works [21], [22, 23].

2.4 Maximum Power Point Tracking (MPPT)

At any speed, from (1)

$$P_m = k_p c_p v_w^3 = k_p c_p \left(\frac{\omega_r}{r_{gear} \lambda} \right)^3 \quad (4)$$

$$\omega_r = r_{gear} \lambda \left(\frac{P_m}{k_p c_p} \right)^{\frac{1}{3}} \quad (5)$$

where ω_t and ω_r [p.u] are the angular speed of the turbine and rotor respectively, and P_m is the turbine mechanical power in [p.u]. The scaling factor k_p ($= \frac{\rho A c_{pmax} \times v_{wBASE}^3}{2 P_{BASE}}$) indicates maximum

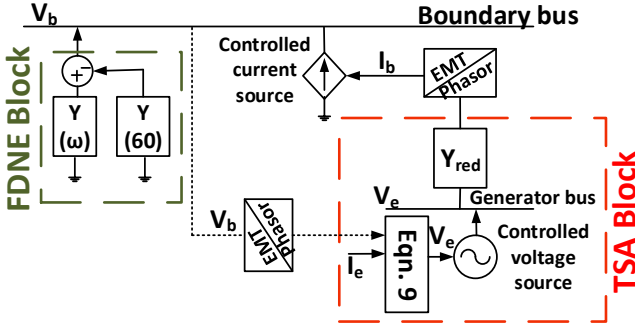


Fig. 2: FDNE and TSA block diagram for a power network.

output power at base wind speed. The angular speed of the turbine, ω_t [p.u], is related to the generator rotor speed by the gear ratio, ($r_{gear} = 1.2$), i.e. $\omega_t = \frac{\omega_r}{r_{gear}}$.

3 Frequency-Dependent Reduced Order Modeling of Power Grid

Large power systems can be modeled as an equivalent to reduce complexity and computational burden while preserving the high and low-frequency behavior of the system under consideration. To this effect, the proposed frequency dependent reduced-order power system models the area of interest (study) area in detail and the remaining part as a combination of FDNE and coherency based TSA equivalent. First, FDNE is formulated based on online RLS identification, by short and open circuiting all voltage and current sources respectively and energizing the external area with constant voltage and varying frequency. The FDNE is represented as a discrete transfer function and rearranged as shown in (6).

$$I_b(k) = -a_1 I_b(k-1) - a_2 I_b(k-2) \cdots - a_n I_b(k-n) + b_1 V_b(k-1) + b_2 V_b(k-2) \cdots + b_n V_b(k-n) \quad (6)$$

where I_b and V_b are the boundary bus current and voltages respectively, k is the current sample and n is the order.

For designing the TSA equivalent and to further reduce the complexity and computational burden, all generating units and nodes in external area are aggregated using coherency based inertial aggregation [24, 25] and the admittance matrix (Y) of external area is reduced to $Y_{red}(2 \times 2)$ matrix by Kron node reduction method represented as follows:

$$\begin{bmatrix} I_b \\ I_e \end{bmatrix} = \begin{bmatrix} Y_{bb} & Y_{be} \\ Y_{eb} & Y_{ee} \end{bmatrix} \begin{bmatrix} V_b \\ V_e \end{bmatrix} \quad (7)$$

where I_e and V_e are the generator bus current and voltage respectively. The generator bus voltage is calculated as shown in (8) and generator bus is energized with V_e as shown in Fig. 2.

$$V_e = [I_e - Y_{eb} V_b] Y_{ee}^{-1} \quad (8)$$

Finally, I_b is calculated as shown in (9) and injected into the boundary bus.

$$I_b = Y_{bb} V_b + Y_{be} V_e \quad (9)$$

The advantage of this method is that the reduced power system model behaves as the original system and can replace the original system for further dynamic assessment of renewable energy sources. Further details regarding reduced order modeling are discussed in [26, 27].

4 Proposed Adaptive Pitch Controller

The proposed adaptive pitch controller involves two steps: 1) Recursive Least Square Identification and 2) Calculating gains of the controller.

4.1 Recursive Least Square Identification

The RLS identification with the process input $u(k)$ and the process output $y(k)$ is performed dynamically at every sample k . The n^{th} order process of the model in z-domain can be represented as

$$\frac{y(k)}{u(k)} = \frac{b_1 z^{-1} + b_2 z^{-2} + \cdots + b_n z^{-n}}{1 + a_1 z^{-1} + a_2 z^{-2} + \cdots + a_n z^{-n}} \quad (10)$$

where a' 's and b' 's are the denominator and numerator coefficients of the transfer function respectively. Let N be the observation window length, then (10) can be rewritten as

$$\begin{bmatrix} y(k) \\ y(k-1) \\ \vdots \\ y(k-N+1) \end{bmatrix}_{N \times 1} = [X_{N \times 2n}] \begin{bmatrix} a_1 \\ \vdots \\ a_n \\ b_1 \\ \vdots \\ b_n \end{bmatrix}_{2n \times 1} \quad (11)$$

Equation (11) can be represented in the generic form as follows

$$\Phi_{model(N \times 1)} = X_{N \times 2n} \Theta_{2n \times 1} \quad (12)$$

where Φ is a matrix of past and current outputs (y), X is a matrix of past inputs and outputs and, Θ is a matrix of the numerator and denominator coefficients of the transfer function. If the identified model is different from measurements, then

$$\epsilon = \Phi_{measured} - \Phi_{model} \quad (13)$$

where ϵ is the error between the measurements from the system (subscript measured) and the identified model (subscript model) for which criteria J can define as

$$J = \epsilon^t \epsilon \quad (14)$$

By letting $dJ/d\Theta = 0$, we get

$$\Theta = [X^t X]^{-1} X^t \Phi_{measured} \quad (15)$$

From (15), to identify the coefficients of the transfer function the inverse of the state matrix should be computed. If the size of the state matrix is large, inverting a large matrix will slow down the process and sometimes may be even not achievable. To overcome this issue, a recursive least squares technique is used. RLS is a computational algorithm that recursively finds the coefficients of the model and eliminates the matrix inversion. Let $S = X^t X$ then (15) can be written as

$$\Theta = S^{-1} X^t \Phi \quad (16)$$

where $\Phi = \Phi_{measured}$

$$\Theta(k) = S^{-1} [x(k) X^t(k-1)] \begin{bmatrix} \Phi(k) \\ \Phi(k-1) \end{bmatrix} \quad (17)$$

$$\Theta(k) = S^{-1} [x(k) \Phi(k) + X^t(k-1) \Phi(k-1)] \quad (18)$$

Using (12)

$$\Theta(k) = S^{-1} [x(k) \Phi(k) + X^t(k-1) X(k-1) \Theta(k-1)] \quad (19)$$

$$\Theta(k) = S^{-1} [x(k)\Phi(k) + S(k-1)\Theta(k-1)] \quad (20)$$

$$S(k) = S(k-1) + x(k)x'(k) \quad (21)$$

Substituting (21) in (20)

$$\Theta(k) = S^{-1} [x(k)\Phi(k) + \{S(k) - x(k)x'(k)\}\Theta(k-1)] \quad (22)$$

$$\Theta(k) = \Theta(k-1) + [S(k-1) + x(k)x'(k)]^{-1}x(k) [\Phi(k) - x'(k)\Theta(k-1)] \quad (23)$$

Let $P(k) = S^{-1}(k)$, and by matrix inversion lemma $P(k)$ can be represented as

$$P(k) = P(k-1) \left[I - \frac{x(k)x'(k)P(k-1)}{1 + x'(k)P(k-1)x(k)} \right] \quad (24)$$

Substituting (21) in (20) and letting

$$K(k) = \frac{P(k-1)x(k)}{1 + x'(k)P(k-1)x(k)} \quad (25)$$

where $P(k)$ can be written as

$$P(k) = [I - K(k)x'(k)] P(k-1) \quad (26)$$

Therefore, (23) can be represented as

$$\Theta(k) = \Theta(k-1) + K(k) [\Phi(k) - x'(k)\Theta(k-1)] \quad (27)$$

With weighted least square, (25) and (26) can be presented as

$$K(k) = \frac{P(k-1)x(k)}{\gamma + x'(k)P(k-1)x(k)} \quad (28)$$

$$P(k) = \frac{[I - K(k)x'(k)] P(k-1)}{\gamma} \quad (29)$$

Finally, using the process input $u(k)$ and process output $y(k)$, the numerator and denominator coefficients of the transfer function (10) can be computed using RLS identification [28].

4.2 Calculating Gains of the Controller

For calculating the gains of the controller, the process model is always restricted to second order. This algorithm calculates the proportional, integral, and derivative gains K_p , K_i , and K_d every sample period. In this process, the closed loop pole shifting factor α is the only adjustment or tuning that is required. Using (10) 2^{nd} order model can be represented as

$$\frac{y}{u} = \frac{b_1q^{-1} + b_2q^{-2}}{1 + a_1q^{-1} + a_2q^{-2}} = \frac{B}{A} \text{ (open loop)} \quad (30)$$

From (27), the open loop characteristic equation is given by

$$1 + a_1q^{-1} + a_2q^{-2} = 0 \quad (31)$$

Thus, the closed loop characteristic equation using pole shifting by a factor α can be represented as

$$(1 + \alpha q^{-1})(1 + a_1\alpha q^{-1} + a_2\alpha^2 q^{-2}) = 0 \quad (32)$$

where, $0 \leq \alpha \leq 1$ and q is a shift operator. From the above, the control structure is given by

$$u(k) = \frac{T(q^{-1})}{R(q^{-1})}y_r(k) - \frac{S(q^{-1})}{R(q^{-1})}y(k) \quad (33)$$

If in (33) we let

$$R(q^{-1}) = (1 - q^{-1})(1 + r_1q^{-1}) \quad (34)$$

$$S(q^{-1}) = s_0 + s_1q^{-1} + s_2q^{-2} \quad (35)$$

where

$$s_0 = T_s K_i + \frac{K_d}{T_s} + K_p$$

$$s_1 = -\frac{2K_d}{T_s} - K_p + r_1 K_p$$

$$s_2 = \frac{K_d}{T_s} - r_1 K_p$$

The architecture can be represented in terms of PID gains, which can be calculated using the following set of equalities:

$$K_i = \frac{-(s_0 + s_1 + s_2)}{T_s} \quad (36)$$

$$K_p = \frac{(s_1 + 2s_2)}{1 + r_1} \quad (37)$$

$$K_d = T_s \left[\frac{r_1 s_1 - (1 - r_1)s_2}{1 + r_1} \right] \quad (38)$$

As the system operating conditions changes, the coefficients of the transfer function get updated and hence the STR PID controller auto-tunes in real-time. The derivative part in PID controller helps in reducing the overshoot. Fig. 3 shows the architecture of the proposed controller.

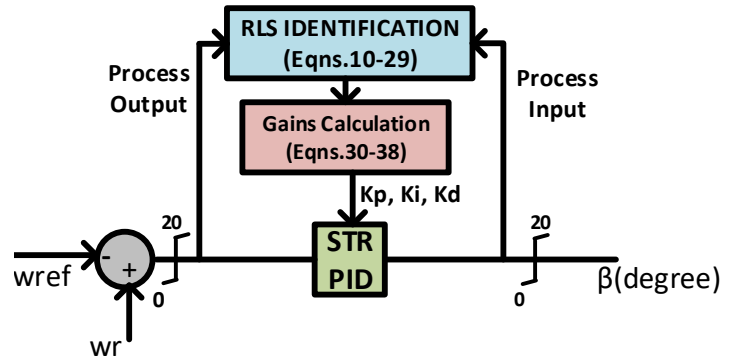


Fig. 3: Proposed STR Controller.

5 Implementation of the Proposed Controller

The proposed adaptive pitch angle controller uses the difference between the reference speed (ω_{ref}) and the actual speed (ω_r) for estimating the control signal. The ω_{ref} is calculated as follows:

Step:1 Initialize ω_r and estimate P_m from (4) and represented as:

$$P_m(t) = k_p c_p \left(\frac{\omega_r(t)}{r_{gear} \lambda} \right)^3 \quad (39)$$

At MPPT, λ , $c_p = 1$ [p.u] and using (39), the mechanical power is represented as

$$P_m(t) = k_p \left(\frac{\omega_r(t)}{r_{gear}} \right)^3 \quad (40)$$

where t is the current iteration.

Step:2 The electrical power delivered P_e is calculated using grid

conditions at boundary and PCC bus to include the grid transient effects in the controller action, whereas conventional pitch controller doesn't account for this calculation.

$$P_e(t) = \frac{V_{pcc}(t)V_B(t)}{X} \sin(\delta_B(t) - \delta_{pcc}(t)) \quad (41)$$

where V_{pcc} and V_B is the voltage of the WTG bus and boundary bus respectively, δ_{pcc} and δ_B are the voltage angle at PCC and boundary bus respectively, and X is the reactance between PCC and boundary bus. Generally, stator resistance is small enough to ignore power loss associated with it and when the converter power loss is neglected, the total real power (here P_e) injected into the grid equals to the sum of the stator power and the rotor power [29, 30].

Step:3 Using the P_m in (40) and P_e in (41), the ω_r is calculated as follows:

$$\omega_r(t+1) = \frac{P_m(t) - P_e(t)}{J \left(\frac{\omega_r(t) - \omega_r(t-1)}{\Delta t} \right)} \quad (42)$$

where J is the moment of inertia, Δt is the simulation time step. Steps 1, 2 and 3 are repeated until P_m and ω_r is converged and the converged value of ω_r is taken as the ω_{ref} (Fig. 4). The integrated implementation flowchart is as shown in Fig. 5.

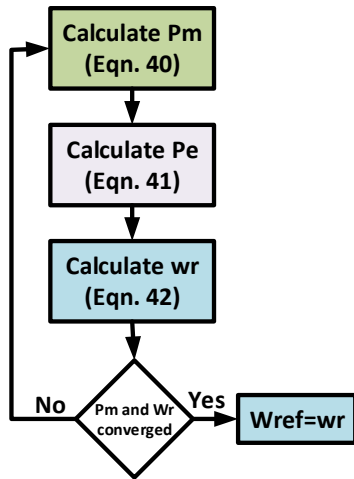


Fig. 4: Flowchart for ω_{ref} calculation.

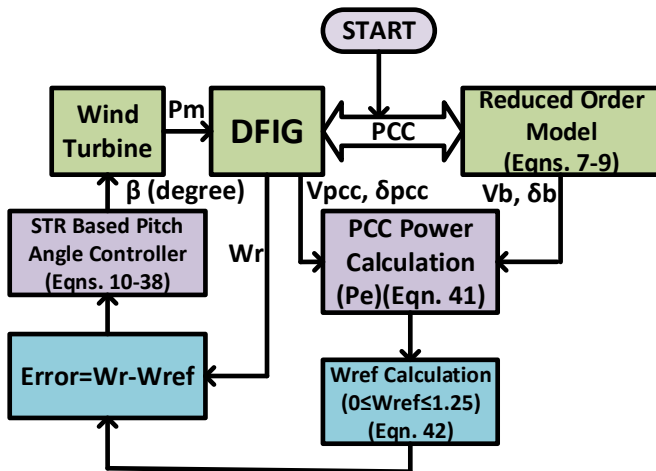


Fig. 5: Flowchart of the proposed controller.

6 Experimental Test Bed and Results

The proposed framework in Fig. 5 is using a lab real-time simulator set up on Kundur's two-area [31] and IEEE 39-bus [32] test system models with WTGs. Table 1 and 2 show the simulation parameters of the wind turbine and DFIG. The real-time test bed consists of a) Reduced order RTDS/RSCAD™ models of Kundur two area and IEEE 39-bus test systems, b) RTDS/RSCAD™ model of WTGs and, c) GTNET-SKT connection between RTDS and MATLAB for interfacing TSA type equivalent with EMT type simulation (Fig. 6). The grid models are an actual representation of the wind farms and characterize real-time closed-loop control with real-life verified generator and control models with GE controllers. The operating principle of the test-bed is the rules that guide the machine model to work based on the grid changes.

Table 1 Simulation Parameters of Wind Turbine)

| Parameter Name | Value |
|--|----------------|
| Rated generator power | 2.2 MVA |
| Rated turbine power | 2.0 MW |
| Generator speed at rated turbine speed (p.u) | 1.2 p.u. |
| Rated wind speed | 12.0 m/s |
| Cut-in wind speed | 6.0 m/s |
| Cut-out wind speed | 25 m/s |
| Rate of change of pitch angle | $\pm 10^0 / s$ |

Table 2 Simulation Parameters of DFIG)

| Parameter Name | Value |
|------------------------------------|--------------|
| Rated stator voltage (L-L RMS) | 0.69 kV |
| Turn ratio (rotor over stator) | 2.6377 |
| Rated MVA | 2.2 MVA |
| Stator resistance | 0.00462 p.u. |
| Stator leakage reactance | 0.102 p.u. |
| Unsaturated magnetizing reactance | 4.348 p.u. |
| First cage rotor resistance | 0.006 p.u. |
| First cage rotor leakage reactance | 0.08596 p.u. |
| Inertia constant | 1.5 MWs/MVA |

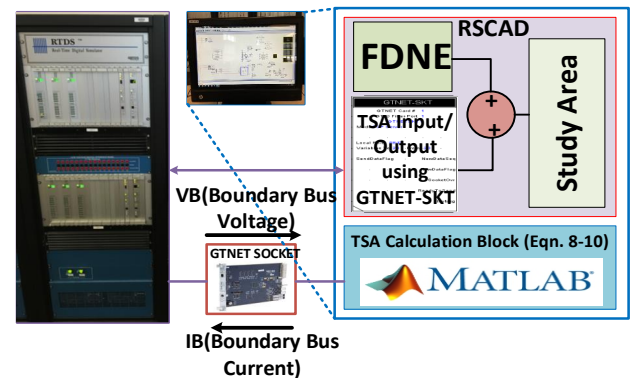


Fig. 6: Experiment setup in RTDS.

6.1 Validation of the algorithm using Kundur's test system

First, for validating the algorithm using grid integrated WTGs, two-area test system (see Fig. 7) is used. The test system consists of four 900MVA synchronous generators and a WTG at bus-10. Based on the location of WTG, the test system is divided into study and

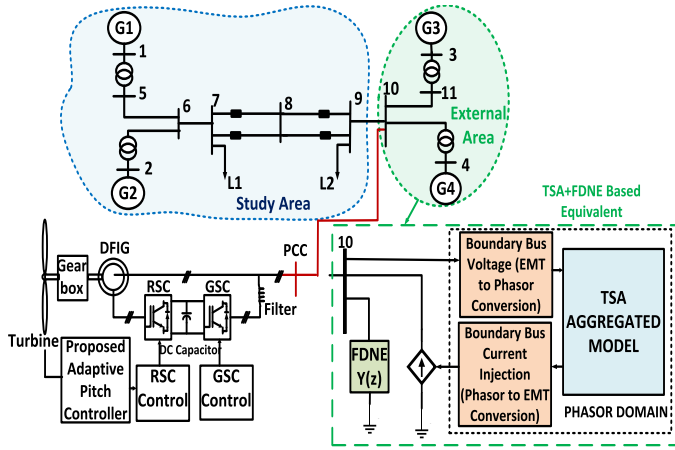


Fig. 7: Proposed dynamic equivalent of two-area test system.

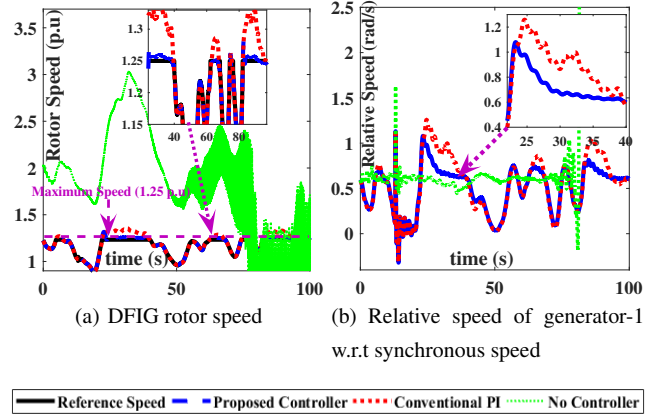


Fig. 10: DFIG rotor speed and relative speed comparison.

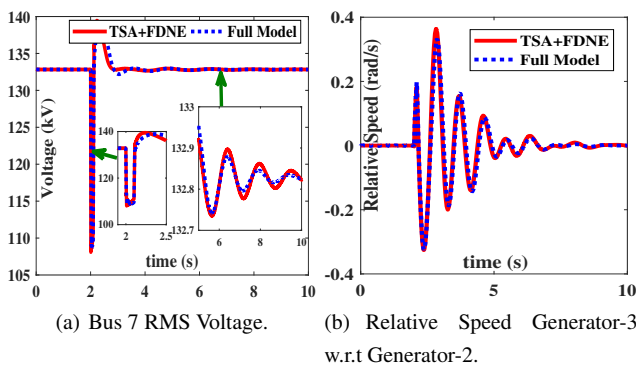


Fig. 8: FDNE validation

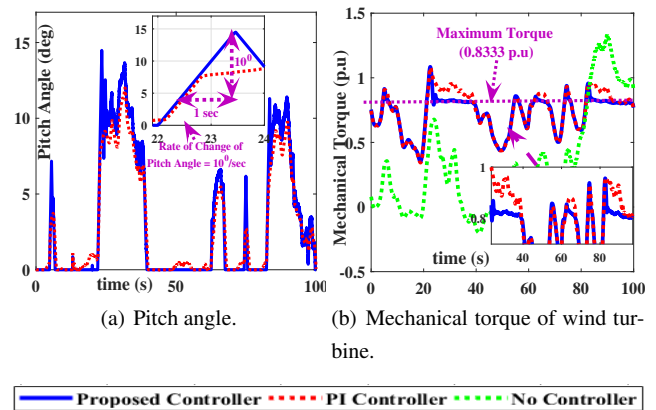


Fig. 11: Pitch angle and mechanical torque comparison.

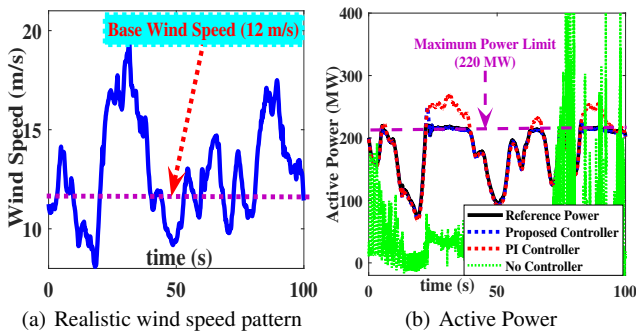


Fig. 9: Wind Speed and DFIG Active Power

external area as shown in Fig. 7. The external area is modeled as a wide-band equivalent, which is the combination of TSA and FDNE. The TSA type equivalent is modeled in MATLAB[®] in phasor domain and FDNE type equivalent is modeled in RSCAD[™] in EMT domain. The reduced order model of the test system is validated by comparing its behavior under transient response with the original test system. For this, 3-phase bolted fault is created at 0.1 sec for the duration of 0.1 sec. Fig. 8(a) and Fig. 8(b) shows the comparison of RMS voltage at bus 7 and the relative speed of Gen-3 w.r.t Gen-2 respectively. From the above results, it can be observed that the reduced order model behaves similarly as the full model under transient condition. Several other event analyses have been studied and similar results are obtained.

To validate the controller under rapidly varying realistic wind conditions Fig. 9(a) has been extracted from the ERCOT data along with a 3-phase bolted fault on Bus-8 for a duration of 6 cycles at 13

sec, and the performance is compared with conventional PI and no controller systems. Figs. 9(b)-10(a) show the active power and rotor speed of the DFIG. It shows that with conventional controller the rating of the DFIG exceeds its limit and effectively increases stress on all connected electrical equipment. For example, the active power at 30sec with a proposed controller is 219.6 MW, whereas with a conventional controller it is 264.06 MW. So, with the conventional controller, the active power is 20% more than the rated value which increases the stress on electrical equipment. Even the rotor speed crosses its limit when controlled by conventional PI controller (For example, it crosses 1.35 p.u at 30 sec while the limit is 1.25 p.u). So it can be concluded that the proposed controller controls the output power and at the same time limits the rotor speed. Additionally, other conventional generators (for example G_1 here) connected to the grid has less rotor oscillations with proposed controller (See Fig. 10(b)). Also, it can be seen from Fig. 11(a) that the rate of change of pitch angle is within its limit (10 deg/s). Additionally, Fig. 11(b) illustrates that the proposed controller is effectively limiting the mechanical torque. It can be observed that at 90 sec the mechanical torque with a conventional controller is 0.9266 p.u. Hence, the conventional controller provides fatigue caused by increased mechanical stress on the turbine due to torque overrun by 11.20%. The RLS identification is performed for $\omega_r - \omega_{ref}$ and β as shown in Fig. 3. The controller gains K_i , K_p , and K_d are calculated at every time step using online identification routine. The conventional PI controller gains are adapted from GE wind turbine field implemented values [4].

Fig. 12 shows the comparison of gains of STR and conventional PI controller for two-area system. From Fig. 12, it can be seen that STR controller auto-tunes as the operating condition changes whereas conventional PI controller has fixed gains irrespective of operating condition. For reliable operation, the generator should be

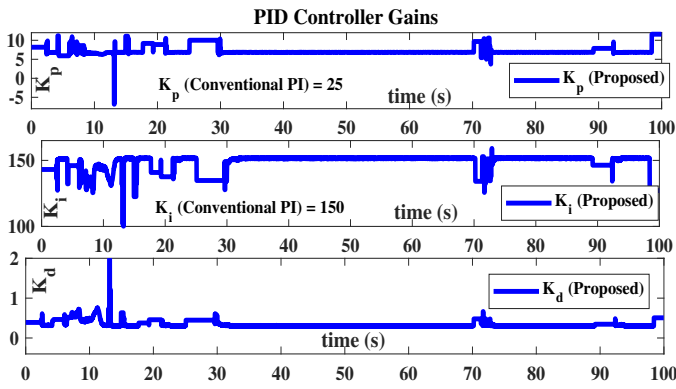


Fig. 12: STR and conventional PI controller gains.

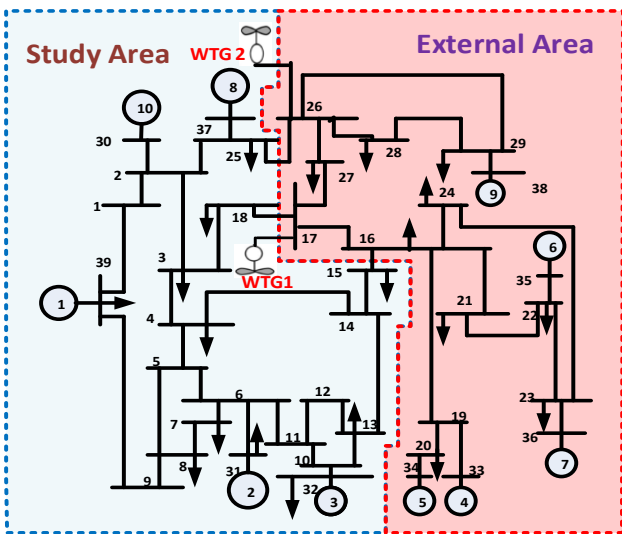


Fig. 13: IEEE 39-Bus system.

operated below the maximum speed limit (1.25 p.u) and thus tuning is necessary.

6.2 Validation of the algorithm with IEEE 39-bus test system

For further validation, the algorithm is also implemented on IEEE 39-bus system with WTGs connected at bus 17 and bus 26. The test system is divided into study and external area based on the location of the WTGs as shown in Fig. 13. The external area is modeled as a combination of TSA and FDNE.

In this case, the proposed controller is tested and validated for variable wind speed pattern (Fig. 14(a)) along with a 3-ph bolted fault on Bus-14 for 0.1 sec at 13sec. With the proposed controller, PCC voltage is much smoother and within allowable limit during high wind speed conditions when compared to PCC voltage with conventional PI controller (Fig. 14(b)). For example, the voltage at 40sec with the proposed controller is 1.017 p.u, whereas with a conventional controller, the voltage is 0.9692 p.u. So, with the conventional controller, the voltage is 6.266% less than the steady state value (1.034 p.u). Hence, the proposed controller improves the voltage by 4.93% and can keep the voltage at the PCC within stable regions during high wind speed conditions. Fig. 15(a) shows the comparison of DFIG rotor speed of WTG-2 and Fig. 15(b) shows the comparison of the active power of WTG-1. Fig. 16(a) shows the relative speed of synchronous generator-3. Fig. 16(b) shows the mechanical torque of WTG-2.

It can be seen that, the active power at 45sec with proposed controller is 218.7 MW, whereas with a conventional controller it is 285.8 MW. So, with the conventional controller, the active power is 29.9% more than the rated value which increases the stress on electrical equipment. Also, the rotor speed crosses its limit using conventional controller (for example, it crosses 1.37p.u at 45 sec where the limit is 1.25 p.u). The WTG control helps to keep the speed and active power under control and yet can keep the voltage at the PCC and other buses within stable operating region during high wind speed conditions. It can be observed that at 40 sec the mechanical torque with conventional controller is 0.9968 p.u, so the conventional controller provides fatigue caused by increased mechanical stress on the turbine due to torque overrun by 19.62%.

Hence, with the proposed controller, during high wind speed conditions, all electrical and mechanical parameters are within the rated limits so actions that are otherwise required to protect the electrical and mechanical equipment during these conditions is not a primary concern. Further with the proposed controller synchronous machine oscillations in the grid are damped out much faster when compared

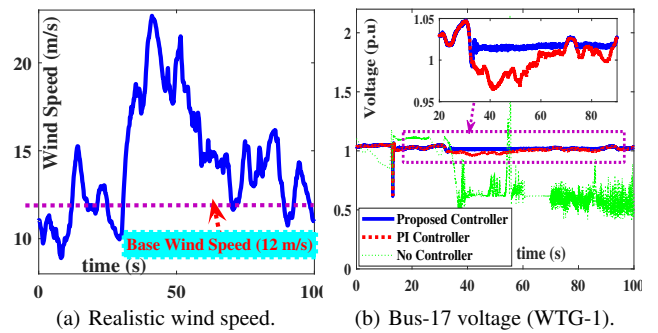


Fig. 14: Wind speed and PCC voltage comparison.

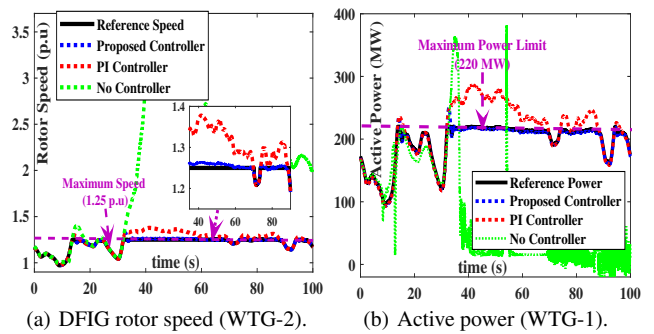


Fig. 15: DFIG rotor speed and active power comparison.

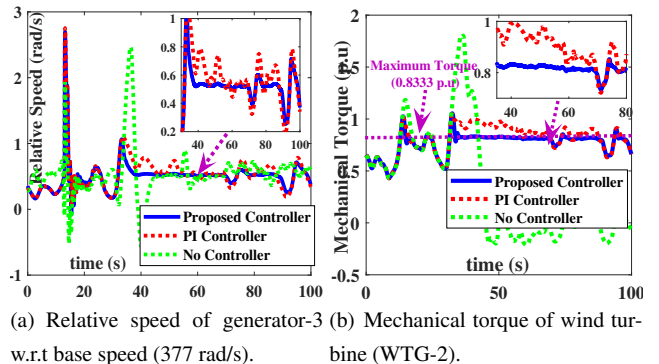


Fig. 16: Relative speed and mechanical torque comparison.

to conventional PI controller. The proposed architecture also ensures that the active power transfer is smooth thus maintaining the required power balance during high wind speed conditions.

7 Conclusion

The proposed sensor-less pitch angle control of WTG, considering the grid dynamics at wide band frequency and using STR controller is an efficient way of controlling the speed of the turbine during high wind speed. WTG is connected to reduced order model of power grid, the area in which WTG connected is modeled in detail while the remaining part is modeled as a combination of FDNE and coherency based TSA equivalent. The proposed method is validated in RTDS/RSCAD using WTG integrated reduced order models of Kundur two-area and IEEE-39 bus test systems. The results clearly illustrate that the proposed pitch angle controller provides better power balance, voltage regulation and reduces fatigue on the turbine. Additionally, the proposed architecture can work without anemometer, thus avoiding any kind of malfunctioning of the device. It has also been demonstrated that the architecture can be implemented in real-life as demonstrated using real-time simulators.

8 References

- 1 'Electricity in the united states'. (. Available from: https://www.eia.gov/energyexplained/index.cfm?page=electricity_in_the_united_states
- 2 Alhmod, L.: 'Reliability improvement for high-power igbt in wind energy applications', *IEEE Trans Ind Electron*, 2018, **PP**, pp. 1–9
- 3 Zhang, J., Cheng, M., Chen, Z., Fu, X.: 'Pitch angle control for variable speed wind turbines'. In: Proc. 3rd Int. Conf. Elect. Utility DRPT. (Nanjing, China, 2008, pp. 2691–2696
- 4 Ghosh, S., Kamalasadana, S., Senroy, N., Enslin, J.: 'Doubly fed induction generator (dfig)-based wind farm control framework for primary frequency and inertial response application', *IEEE Trans Power Syst*, 2016, **31**, pp. 1861–1871
- 5 Zhang, Y., Gole, A.M., Wu, W., Zhang, B., Sun, H.: 'Development and analysis of the applicability of a hybrid transient simulation platform combining tsa and emt elements', *IEEE Trans Power Syst*, 2013, **28**, pp. 357–366
- 6 Wang, S., Lu, S., Zhou, N., Lin, G., Elizondo, M., Pai, M.A.: 'Dynamic-feature extraction, attribution, and reconstruction (dear) method for power system model reduction', *IEEE Trans Power Syst*, 2014, **29**, pp. 2049–2059
- 7 Liang, Y.F., Lin, X., Gole, A.M., Yu, M.: 'Improved coherency based wide-band equivalents for real-time digital simulators', *IEEE Trans Power Syst*, 2011, **26**, pp. 1410–1417
- 8 Zhang, Y., Cheng, M., Chen, Z.: 'Load mitigation of unbalanced wind turbines using pi-r individual pitch control', *IET Renewable Power Generation*, 2015, **9**, pp. 262–271
- 9 Van, T.L., Nguyen, T.H., Lee, D.C.: 'Advanced pitch angle control based on fuzzy logic for variable-speed wind turbine systems', *IEEE Trans Energy Convers*, 2015, **30**, pp. 578–587
- 10 Lasheen, A., Elshafei, A.L.: 'Wind-turbine collective-pitch control via a fuzzy predictive algorithm', *Renewable Energy*, 2016, **87**, pp. 298–306
- 11 Ren, Y., Li, L., Brindley, J., Jiang, L.: 'Nonlinear pi control for variable pitch wind turbine', *Control Engineering Practice*, 2016, **50**, pp. 84–94
- 12 Das, K.K., Buragohain, M.: 'An algorithmic approach for maximum power point tracking of wind turbine using particle swarm optimization', *IJAREEIE*, 2015, **4**, pp. 4099–4106
- 13 Soued, S., Ebrahim, M.A., Ramadan, H.S., Becherif, M.: 'Optimal blade pitch control for enhancing the dynamic performance of wind power plants via metaheuristic optimisers', *IET Electric Power Application*, 2017, **11**, pp. 1432–1440
- 14 Thakallapelli, A., Ghosh, S., Kamalasadana, S.: 'Real-time reduced order model based adaptive pitch controller for grid connected wind turbines'. In: Proc. IEEE Industry Applications Society Annual Meeting. (Portland, USA, 2016, pp. 1–8
- 15 Ghosh, S., Senroy, N.: 'Electromechanical dynamics of controlled variable speed wind turbines', *IEEE Syst Journal*, 2015, **9**, pp. 639–646
- 16 'Wind-turbine driven doubly-fed induction generator user manual'. (. 2015
- 17 Slootweg, J.G., de Haan, S.W.H., Polinder, H., Kling, W.L.: 'General model for representing variable speed wind turbines in power systems dynamics simulations', *IEEE Trans Power Syst*, 2003, **18**, pp. 144–151
- 18 Chen, J., Lin, T., Wen, C., Song, Y.: 'Design of a unified power controller for variable-speed fixed-pitch wind energy conversion system', *IEEE Trans Ind Electron*, 2016, **63**, pp. 4899–4908
- 19 Chen, J., Chen, J., Gong, C.: 'New overall power control strategy for variable-speed fixed-pitch wind turbines within the whole wind velocity range', *IEEE Trans Ind Electron*, 2013, **60**, pp. 2652–2660
- 20 'Wind turbine, documentation simpowersystems'. (. 2004
- 21 Pena, R., Clare, J.C., Asher, G.M.: 'Doubly fed induction generator using back-to-back pwm converters and its application to variable speed wind-energy generation'. In: IEE Proceedings - Electric Power Applications. (. 1996, pp. 231–241
- 22 Gole, A.: 'Vector controlled doubly fed induction generator for wind applications'. (. 2004
- 23 Woodford, D.A.: 'Determination of main parameters for a doubly fed induction generator for a given turbine rating'. (. 2004
- 24 Thakallapelli, A., Hossain, S.J., Kamalasadana, S.: 'Coherency based online wide area control of renewable energy integrated power grid'. In: Proc. IEEE PEDES. (Trivandrum, India, 2016, pp. 1–6
- 25 Chow, J. H.: 'Power System Coherency and Model Reduction'. Power Electronics and Power Systems. (Springer New York, 2014). Available from: <https://books.google.com/books?id=HGnABAAQBAJ>
- 26 Thakallapelli, A., Ghosh, S., Kamalasadana, S.: 'Real-time frequency based reduced order modeling of large power grid'. In: Proc. Power and Energy Society General Meeting. (Boston, USA, 2016, pp. 1–5
- 27 Thakallapelli, A., Kamalasadana, S.: 'Optimization based real-time frequency dependent reduced order modeling of power grid'. In: Proc. Power and Energy Society General Meeting. (Chicago, USA, 2017, pp. 1–5
- 28 K. J. Astrom and B. Wittenmark: 'Adaptive control'. (Addison-Wesley Publishing Company, 1995)
- 29 Lei, Y., Mullane, A., Lightbody, G., Yacmini, R.: 'Modeling of the wind turbine with a doubly fed induction generator for grid integration studies', *IEEE Trans Energy Convers*, 2006, **21**, pp. 257–264
- 30 Muller, S., Deicke, M., Doncker, R.W.D.: 'Doubly fed induction generator systems for wind turbines', *IEEE Ind Appl Mag*, 2002, **8**, pp. 26–33
- 31 P. Kundur: 'Power System Stability and Control'. (New York: McGraw-Hill, 1994)
- 32 Hiskens, I.: 'Report: 39-bus system (new england reduced model)'. (. 2013